

Hybrid Local-Global Transformer for Image Dehazing

Dong Zhao¹, Jia Li^{*1,2,3}, Hongyu Li¹, and Long Xu^{2,3}

¹State Key Laboratory of Virtual Reality Technology and Systems, SCSE, Beihang University.

²Key Laboratory of Solar Activity, National Astronomical Observatories, Chinese Academy of Sciences, Beijing 100012, China.

³Peng Cheng Laboratory, Shenzhen 518000, China.

Abstract

Recently, the Vision Transformer (ViT) has shown impressive performance on high-level and low-level vision tasks. In this paper, we propose a new ViT architecture, named Hybrid Local-Global Vision Transformer (HyLoG-ViT), for single image dehazing. The HyLoG-ViT block consists of two paths, the local ViT path and the global ViT path, which are used to capture local and global dependencies. The hybrid features are fused via convolution layers. As a result, the HyLoG-ViT reduces the computational complexity and introduces locality in the networks. Then, the HyLoG-ViT blocks are incorporated within our dehazing networks, which jointly learn the intrinsic image decomposition and image dehazing. Specifically, the network consists of one shared encoder and three decoders for reflectance prediction, shading prediction, and haze-free image generation. The tasks of reflectance and shading prediction can produce meaningful intermediate features that can serve as complementary features for haze-free image generation. To effectively aggregate the complementary features, we propose a complementary features selection module (CFSM) to select the useful ones for image dehazing. Extensive experiments on homogeneous, non-homogeneous, and nighttime dehazing tasks reveal that our proposed Transformer-based dehazing network can achieve comparable or even better performance than CNNs-based dehazing models.

1. Introduction

In bad weather conditions (such as haze, mist, and fog), the captured outdoor images are usually degraded by the small particles or water-droplets suspended in the atmosphere [32]. Due to the atmospheric scattering, emission,

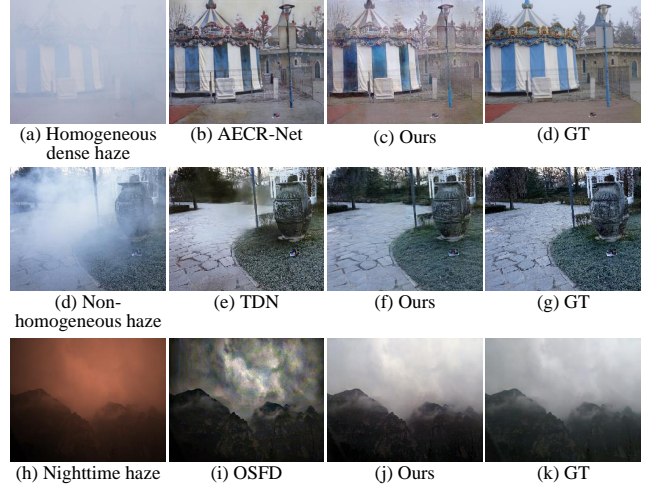


Figure 1. Visual comparisons with the state-of-the-arts on homogeneous, non-homogeneous, and nighttime dehazing. (b), (f), and (i) are the results of AECR-Net [41], TDN [27], and OSFD [45], respectively.

and absorption, the degraded images suffer from the *color* distortion and *texture* blurring [14]. Early prior-based single image dehazing methods use handcrafted priors that are observed from the *color* information, such as dark channel prior (DCP) [17], color attenuation prior (CAP) [49] and haze-line prior (HLP) [5], and the *texture* information, such as change of detail prior [23]. However, when the priors are invalid in some instances, these methods may generate unnatural artifacts.

It has witnessed the rapid development of deep learning in recent years, and many CNNs-based image dehazing methods have been proposed to estimate the haze effects. These methods commonly outperform the prior-based method since the deep networks can implicitly learn the rich haze-relevant features and overcome the limitations of a single specific prior [24]. However, existing CNNs-based de-

*Corresponding author: Jia Li (jjiali@buaa.edu.cn).

hazing models suffer from two essential issues stem from two aspects: the convolution layers and the dehazing framework. To the first aspect, on the one hand, convolution is content-independent as the same convolution kernel is shared to the entire image, ignoring the distinct nature between different image regions [31]. On the other hand, due to the inductive biases such as locality, the convolutions are ineffective to learn long-range dependency information [47, 26].

As to the second aspect, existing CNNs-based dehazing methods can be divided into two categories. The first is the physical-based frameworks, such as DehazeNet [6] and multi-scale CNN model (MSCNN) [35], which try to predict the transmission map t and atmospheric light A at the first step, and then use them to calculate the scene radiance J according to the atmospheric scattering model [30] $J(p) = (I(p) - A)/t(p) + A$, where the I is the hazy image, and p is the pixel position. However, the atmospheric scattering model cannot completely represent the complex hazy imaging process since it ignores the emission and absorption of atmospheric particles. Another category is fully data-driven learning-based [24], including enhanced Pix2pixHD dehazing network (EPDN) [35], domain adaptation dehazing network (DADN) [37], multi-scale boosted dehazing network (MSBDN) [13]. Trained in an end-to-end fashion, these models directly recover the haze-free image. However, they have limitations in interpretability [24] and usually appear ineffective in dense haze removal. The above discussions inspire us to use a more powerful mechanism and provide a new framework for image dehazing.

Very recently, Vision Transformers (ViT) [15] have received increasing research interest due to its content-dependent interactions [38] and flexibility in modeling long-range dependencies [10]. However, the quadratic increase in complexity with image size hinders its application on dehazing tasks, which requires high-resolution feature maps. Additionally, it is undeniable that global and local information aggregation are both useful for low-level vision tasks, while the ViT does not possess the locality [15]. To these ends, we propose a Hybrid Local-Global Vision Transformer (HyLoG-ViT), which consists of two paths, the local and global ViT paths. In the local ViT path, the standard ViT blocks are operated in a grid of non-overlapped regions, enabling the ViT model to focus on capturing the fine-grained and short-distance information within the local region. In the global ViT path, one ViT block is operated on the downscaled feature maps to capture the global and long-range dependencies. Then, the hybrid features from the two paths are fused by a convolution layer, improving the local continuity. Compared with the vanilla ViT architecture, the HyLoG-ViT has lower computational complexity and brings locality mechanisms to the networks.

Incorporating with the HyLoG-ViT, we build the dehaz-

ing network based on the motivations that, *color* and *texture* perceptions are the critical visual cues toward identifying objects and understanding scene [48, 19]. For this purpose, we propose a novel approach to jointly learn intrinsic image decomposition and haze removal from single image. It consists of one shared encoder and three parallel decoders for reflectance prediction, shading prediction, and haze-free image generation. Since the reflectance component possesses the true *color* of the scenes [4], it encourages the reflectance prediction subnetwork to learn more intermediate features, which are helpful to restore accurate color information from the degraded images. Furthermore, those intermediate features can be served as complementary features to the dehazing subnetwork and thus improve the dehazing results with high color contrast, as illustrated in Fig. 1. Similarly, the shading prediction subnetwork can provide rich complementary features beneficial to texture enhancement and thus improve the dehazing results with fine details. However, directly aggregate the redundant, complementary features is inefficient as there may have some haze-irrelevant features. To this end, we further propose a Complementary Features Selection Module (CFSM) to automatically select the ‘right’ features that are helpful to dehazing tasks.

The main contributions of this work are:

- We propose a new variant of ViT, namely Hybrid Local-Global Vision Transformer (HyLoG-ViT), which can model both local and global dependencies with lower computational cost than the vanilla ViT. With the HyLoG-ViT, we propose a Transformer-based dehazing network for the first time.
- We build a new dehazing framework that jointly learns the intrinsic image decomposition and image dehazing. The reflectance and shading prediction tasks provide rich complementary features for the haze-free image generation task, enabling the network to generate high-quality haze-free images with natural color and fine details.
- To effectively fuse the complementary features, we propose a Complementary Features Selection Module (CFSM). The CFSM considerably improves the effectiveness of feature aggregation by adaptively enhancing the proper complementary feature channels while weakening the irrelevant ones.

2. Related Work

2.1. Single Image Dehazing

Single image dehazing is an ill-posed problem. Without any auxiliary information, previous dehazing algorithms require the introduction of specific prior knowledge. Through

research in the last decade, many priors have been proposed based on the cues of color, such as the color-line prior [16], CAP [49], and HLP [5], and texture, such as change of detail prior [23].

Recently, CNNs-based dehazing networks have been extensively studied. One kind of CNNs-based network restores the clear image by estimating the intermediate variables in the atmospheric scattering model [30] and then calculates the clear image. For example, the multi-scale CNNs dehazing model [35] utilizes a coarse-scale network to estimate the complete transmission map and use a fine-scale network to refine the results. More recent CNNs-based networks tend to learn hazy-to-clear image translation directly [41]. For example, the MSBDN [13] incorporates boosting and error feedback principles into a U-Net [36] architecture with a dense feature fusion module.

Different from the previous dehazing networks, our dehazing network jointly learns the intrinsic image decomposition and image dehazing. The tasks of reflectance and shading predictions provide rich color and texture complementary features to the dehazing subnetworks, enabling it yields haze-free images with natural color and fine details.

2.2. Vision Transformer

Very recently, Vision Transformers (ViT) [15] have received increasing research interest in image and video vision tasks, including object detection [8], image classification [15] and semantic segmentation [47].

Many new versions of vision transformers have been proposed to relieve the high computational cost problems. For example, the Pyramid Vision Transformer (PVT) [39] applies transformers on lower resolution features which significantly reduces the computational cost. Another workaround, as proposed in the Swin Transformer [29], is the locally-grouped self-attention [10], where the input features are separated into a grid of non-overlapped windows and the vision transformer is operated only within each window. Many methods have been proposed to bring inductive biases into ViT. LocalViT [25] brings a locality mechanism to ViT by employing the depth-wise convolution into the feed-forward network. CvT [42] proposes a convolutional token embedding to model local spatial contexts and a convolutional projection layer to provide efficiency benefits.

2.2.1 Low-level Vision

The IPT [9] employs the standard Transformer directly to low-level tasks. Thus, this model needs to be pre-trained on a large-scale datasets. The Uformer [40] designs a general U-shaped Transformer-based structure for image restoration. It also proposes a locally-enhanced window (LeWin) Transformer block to reduce the computation cost. The SwinIR [26] utilizes residual Swin Transformer blocks to

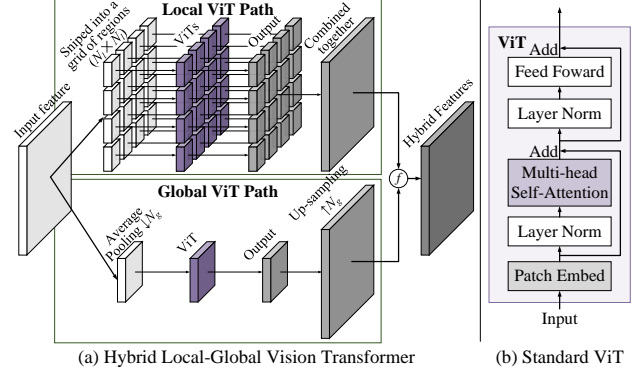


Figure 2. Diagram of the hybrid local-global vision transformer (HyLoG-ViT). \oplus represents the fuse operation.

extract deep features for image restoration.

In our HyLoG ViT, the local ViT path is similar to the LeWin transformer proposed in Uformer. However, using the local version ViT alone fails to model global dependencies and preserve the local continuity around those regions. By contrast, our HyLoG ViT block can capture local and global dependencies simultaneously.

3. Method

3.1. HyLoG-ViT

We propose a Hybrid Local-Global Vision Transformer (HyLoG-ViT) model to address the challenges of high computation cost and lack of locality. As shown in Fig. 2, a HyLoG-ViT block consists of two paths. In the local ViT path, the input feature map is grouped into grids of non-overlapped regions (windows), and the ViT is applied only within each region. Given the feature maps $X \in \mathbb{R}^{H \times W \times C}$ where the H , W and C are the height, width and channel number of the maps, the computation of the local ViT path can be expressed as:

$$\begin{aligned} X &= \{X^1, X^2, \dots, X^{N_l}\}, \quad N_l = HW/M^2; \\ X_l^i &= Vit(X^i), \quad i \in [1, 2, \dots, N_l]; \\ X_l &= \{X_l^1, X_l^2, \dots, X_l^{N_l}\}, \end{aligned} \quad (1)$$

where X_l^i is the output of the i -th region, X_l is the combined output of the local ViT path; $Vit(\cdot)$ represents the standard ViT block. This design enables ViT to focus on capturing region-level attention and explore local context information. However, the local ViT path cannot model global dependencies and lose local continuity around those regions. Therefore, we also introduce the global ViT path, where the input feature is down-sampled by the average pooling operation to reduce the spatial resolution. The output is feed into the standard ViT. The computation of the global ViT path is:

$$X_g = Upsamp(Vit(Avepool(X))); \quad (2)$$

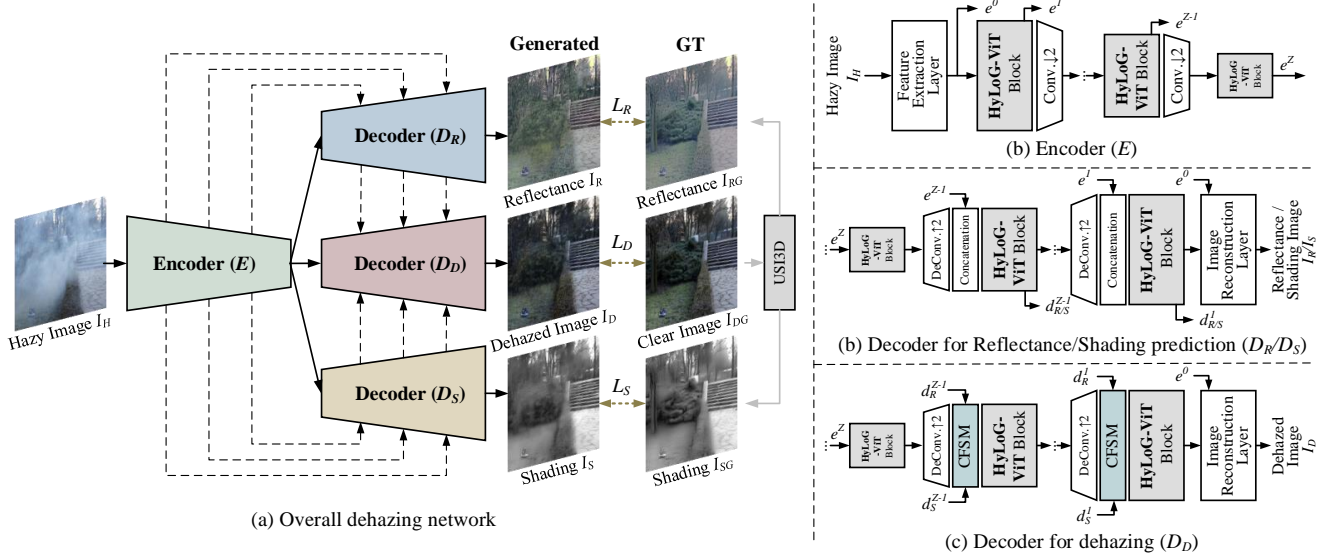


Figure 3. Architectures of our dehazing network. (a): the overall dehazing network, which consists of an encoder and three different decoders. (b): the architecture of the shared encoder E . (c): the architecture of decoder D_R/D_S . (d): the architecture of decoder D_D . USI3D: a pre-trained unsupervised intrinsic image decomposition model proposed by [28]. CFSM: the complementary features selection module. L_R , L_S and L_D : loss functions for the three tasks.

where, X_g is the output of the global ViT path. $Avepool(\cdot)$ is the average pooling; $Upsamp(\cdot)$ represents the upsampling. The global ViT path improves efficiency while still maintaining the capability of aggregating global information. The hybrid outputs of the two paths are concatenated and transformed to the original dimension by a 3×3 convolution layer:

$$X_h = Conv3 \times 3(Concat(X_l, X_g)); \quad (3)$$

where X_h is the final output of HyLoG-ViT block; $Concat(\cdot)$ is the channel-wise concatenation, $Conv3 \times 3(\cdot)$ is a 3×3 convolution layer. This fuse operation maintains the merits of the local and global ViT and introduces locality into the network.

The positional encoding used in transformers aims to retain positional information. However, for low-level vision tasks, the input images with varying sizes are commonly different from the training ones. As a result, it may lead to decreased performance [11, 43] and break the translation invariance [10]. Note that our model can achieve good results even without additional positional encoding modules. We argue that the 3×3 convolution used in (3) is sufficient to provide positional information for Transformers.

3.2. Dehazing Model

Existing dehazing approaches ignore the interference factors that bring significant challenges to the dehazing performance, such as shadows and variation of the color. To achieve high dehazing performance, we propose a features complement-based framework that jointly learns the intrinsic

image decomposition and dehazing. The algorithm of the intrinsic image decomposition decomposes an image into reflectance and shading. The reflectance component contains the actual color of the scenes, and the shading component contains the structure and texture information [4]. As a result, using reflectance and shading images for color and texture restoration can be favorable.

3.2.1 Overall Architecture

The overview of our dehazing network consists of a shared encoder and three decoders, as illustrated in Fig.3. Denote the hazy image is I_H , the encoder E is used to extract the shallow and deep features:

$$e^0 = F_E^0(I_H), e^z = F_E^z(e^{z-1}), \quad (4)$$

where F_E^0 denotes the feature extraction layer used to extract shallow feature e^0 ; F_E^z denotes z -th stage of encoder E , e^z refers to the deep feature at stage z . $z \in [1, \dots, Z]$, and Z is the total number of stages. Three parallel decoders follow the encoder. Decoders D_R and D_S are used to predict the reflectance and shading of the haze-free image, respectively, and their intermediate features are served as complementary features to the decoder D_D to generate the high-quality haze-free image. The decoders are described as:

$$d_R^Z = F_{D_R}^Z(d_E^Z), d_R^z = F_{D_R}^z(d_R^{z-1}, e^z), \quad (5)$$

$$d_S^Z = F_{D_S}^Z(d_E^Z), d_S^z = F_{D_S}^z(d_S^{z-1}, e^z), \quad (6)$$

$$d_D^Z = F_{D_D}^Z(e^Z, d_R^Z, d_S^Z), d_D^z = F_{D_D}^z(d_D^{z-1}, d_R^z, d_S^z), \quad (7)$$

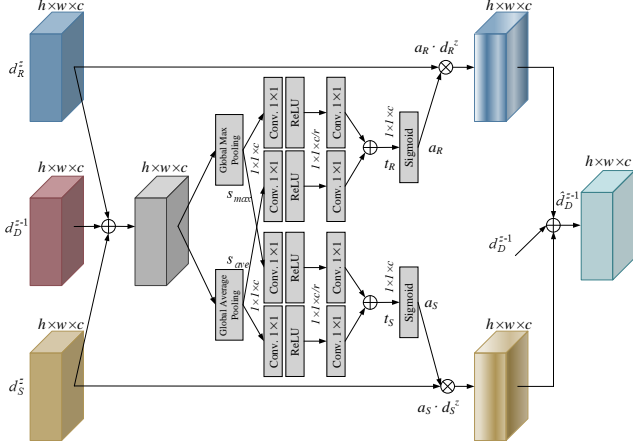


Figure 4. Schematic for the complementary features selection module (CFSM). \oplus denotes the element-wise summation. \otimes denotes the element-wise production.

where $F_{D_R}^z$, $F_{D_S}^z$ and $F_{D_D}^z$ denote the z -th stage of decoder D_R , D_S and D_D , respectively, $z \in [1, \dots, Z]$. d_R^z , d_S^z and d_D^z are the intermediate features of the decoder D_R , D_S and D_D at stage z , respectively. The final reflectance I_R , shading I_S , and haze-free image I_D are generated through three image reconstruction layers, i.e., $F_{D_R}^0$, $F_{D_S}^0$ and $F_{D_D}^0$, respectively. That is:

$$\begin{aligned} I_R &= F_{D_R}^0(d_R^1, e^0), \quad I_S = F_{D_S}^0(d_S^1, e^0), \\ I_D &= F_{D_D}^0(d_D^1, d_R^1, d_S^1, e^0). \end{aligned} \quad (8)$$

3.3. Complementary Features Selection Module

One can simply aggregate the complementary features d_R^z and d_S^z via element-wise summation or concatenation operation, which is inefficient. Therefore, we propose the CFSM to fuse the complementary features in a nonlinear fashion. The architecture of the CFSM is illustrated in Fig.4.

Given the complementary features d_R^z and d_S^z and the feature $d_D^{z-1} (\in \mathbb{R}^{h \times w \times c})$, they are first combined via element-wise summation. Then, the outputs are transformed to two channel-wise statistics s_{ave} and s_{max} ($\in \mathbb{R}^{1 \times 1 \times c}$) by a global average pooling and a global max pooling, respectively. Each statistic is separated into two streams: one stream for d_R^z feature selection, and another for d_S^z . Taking d_R^z stream as an example, the s_{ave} and s_{max} are followed by channel-downscaling 1×1 convolution layers to calculate the compact feature vectors, v_{ave-R} and v_{max-R} ($\in \mathbb{R}^{1 \times 1 \times c/r}$, where $r = 4$ in our model), respectively. The feature vectors are feed into two parallel channel-upscaling 1×1 convolution layers and provides feature descriptors t_{ave-R} and t_{max-R} ($\in \mathbb{R}^{1 \times 1 \times c}$). The final feature descriptor is defined as $t_R = t_{ave-R} + t_{max-R}$.

The t_R passes through the Sigmoid function to generate attention score a_R ($\in \mathbb{R}^{1 \times 1 \times c}$) for d_R^z . Similar, we can get the attention score a_S for d_S^z . The overall process of feature recalibration and aggregation is defined as:

$$\hat{d}_D^{z-1} = d_D^{z-1} + a_R \cdot d_R^z + a_S \cdot d_S^z. \quad (9)$$

3.4. Loss Function

In our training, the ground truths of reflectance I_{GR} and shading I_{GS} are generated by operating the pre-trained intrinsic image decomposition model USI3D [28] on the ground truth of haze-free image I_{GD} . For reflectance and haze-free image estimations, we train the networks using the L2 reconstruction loss and SSIM loss (as used in [7]). For the shading estimation, we use the L2 reconstruction loss and an edge preserve loss which is defined as:

$$\begin{aligned} L_e &= \mathbb{E}_{I_S} [||\nabla_x I_S(p) - \nabla_x I_{SG}(p)||_2 \\ &\quad + ||\nabla_y I_S(p) - \nabla_y I_{SG}(p)||_2], \end{aligned} \quad (10)$$

where \mathbb{E} is the mean operation on a batch of samples; ∇_x and ∇_y are the spatial derivative at x and y directions, respectively. p refers to the spatial location. Overall, the hybrid loss function contains three parts, that is:

$$L = \lambda_R L_R + \lambda_S L_S + \lambda_D L_D, \quad (11)$$

where L_R , L_S , and L_D are the loss functions for the three vision tasks, respectively.

4. Experiment

4.1. Experiment Setup

4.1.1 Dataset

Our dehazing model is trained on outdoor datasets, including RESIDE dataset [22], NTIRE2020-Dehaze dataset [1], and NHR dataset [45], for homogeneous haze, non-homogeneous haze, and nighttime haze removal, respectively. For RESIDE dataset, we randomly select 41240 samples from OTS [22] (outdoor training subset in RESIDE) for training, and 500 samples from SOTS [22] (synthetic objective testing subset in RESIDE) for testing. For NTIRE2020-Dehaze dataset, we synthetic 9800 samples augmented from 50 original high-resolution samples by randomly crop, flip, and rotate; and the 41~45-th samples are used for qualitative evaluations (as set in TDN [27]). The NHR dataset contains 17900 samples, and for fair comparing, we select the last 897 for testing and others for training as set in OSFD [45]. We also collect 200 and 150 real-world daytime and nighttime hazy images to evaluate the performance of our model.

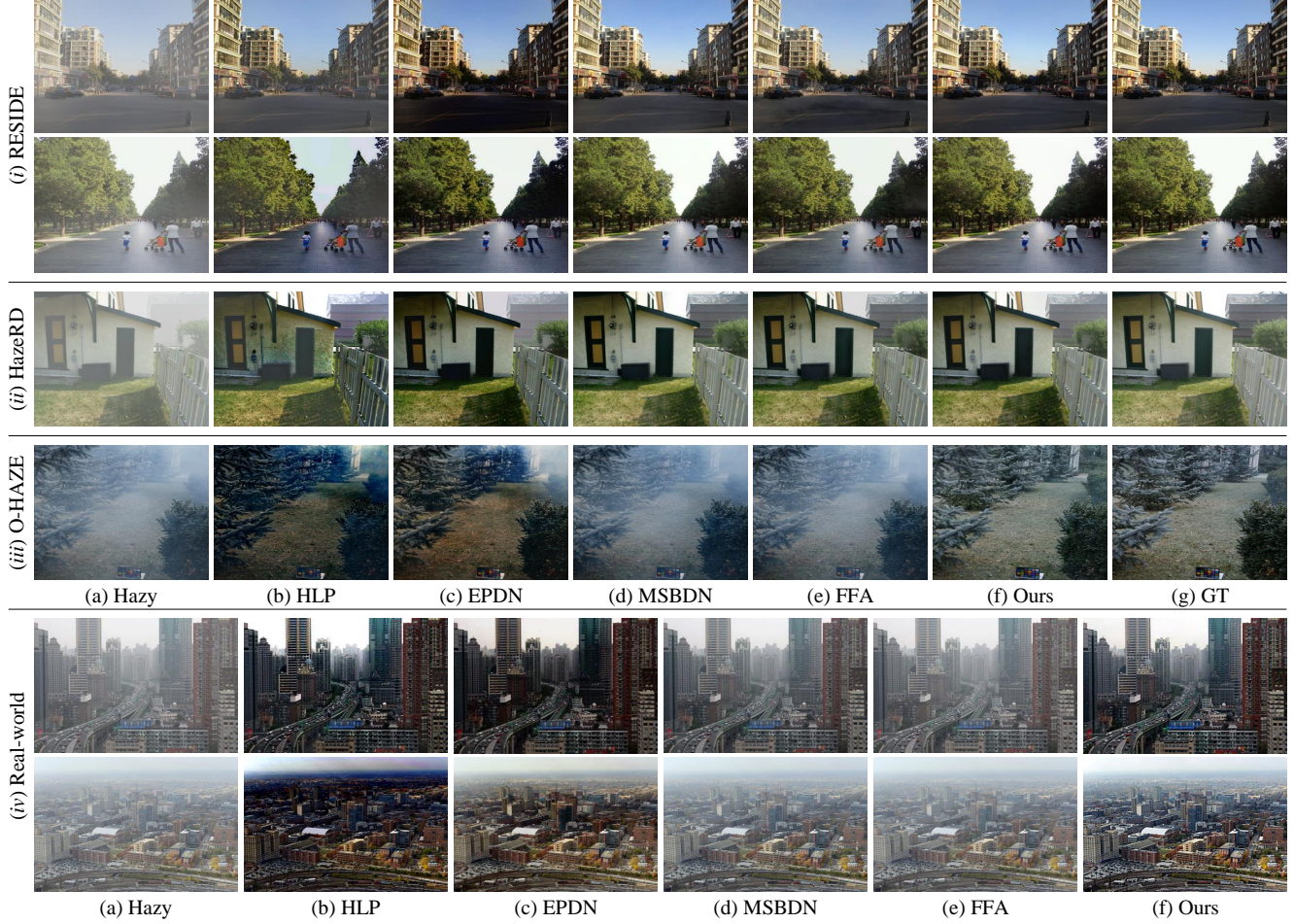


Figure 5. Visual results of homogeneous image dehazing.

4.1.2 Implemental Details

Our dehazing model is implemented with PyTorch library and trained on one NVIDIA GeForce RTX 3090 GPU for 15 epochs. We adopt Adam [20] optimizer with the initial learning rate is 10^{-4} for both CNN and ViT backbones. We use the layer normalization [3] in the ViT block, and Activation Normalization [21] in CNN layers. The parameters of the loss functions are set as $(\lambda_R, \lambda_S, \lambda_D) = (1, 1, 1.5)$.

4.2. Comparisons with State-of-the-art Methods

4.2.1 Homogeneous Dehazing

To demonstrate the effectiveness of our dehazing model on homogeneous image dehazing, we firstly evaluate it on the synthetic datasets, including SOTS (outdoor), HazeRD, and O-HAZE datasets. It can be found from Fig.5(i)-(iii), although most of the compared approaches can provide visually pleasant dehazed results on the SOTS dataset, they fail to recover haze-free images effectively on the other two challenging datasets, either lead to color distortion and

over-saturation results (such as HLP) or remain haze at distant scenes (such as EPDN, MSBDN and FFA [33]). MSBDN and FFA obtain the top two scores on the SOTS dataset, while our model achieves good visual perception and obtains the top two LPIPS [46] scores. Additionally, our model obtains the highest scores of PSNR, SSIM, LPIPS, and DISTs [12] on HazeRD and O-HAZE datasets.

We further evaluate our method on the real-world datasets. The visual comparisons are shown in Fig.5(iv). HLP tends to yield over-enhanced visual artifacts. The CNNs-based methods can avoid the over-enhancement results, but the MSBDN and FFA produce insufficient dehazing in distant scenes. Our dehazing results on real-world hazy images maintain plausible visual details, achieving more remarkable performance than others. As shown in Table 1, our model obtains the second-best BCEA- e and s and the best n metrics, demonstrating that our network can achieve comparable performance to CNNs-based dehazing methods.



Figure 6. Visual results of non-homogeneous dehazing.

SOTS	HLP	EPDN	MSBDN	FFA	Our
PSNR \uparrow	16.443	27.42	33.79	<u>33.38</u>	32.17
SSIM \uparrow	0.784	0.946	0.985	<u>0.980</u>	0.970
LPIPS \downarrow	0.140	0.060	0.038	0.043	<u>0.041</u>
DISTS \downarrow	0.108	0.039	0.016	<u>0.030</u>	0.033
HazeRD	HLP	EPDN	MSBDN	FFA	Our
PSNR \uparrow	15.03	15.762	15.64	<u>16.09</u>	17.39
SSIM \uparrow	0.601	0.608	0.624	<u>0.667</u>	0.706
LPIPS \downarrow	0.284	0.243	0.235	<u>0.232</u>	0.224
DISTS \downarrow	0.174	<u>0.132</u>	0.155	0.152	0.085
O-HAZE	HLP	EPDN	MSBDN	FFA	Our
PSNR \uparrow	15.28	<u>17.17</u>	16.76	16.09	29.87
SSIM \uparrow	0.466	<u>0.600</u>	0.460	0.465	0.920
LPIPS \downarrow	0.306	<u>0.285</u>	0.318	0.323	0.155
DISTS \downarrow	0.226	<u>0.166</u>	0.251	0.261	0.088
RW	HLP	EPDN	MSBDN	FFA	Our
BCEA- $e\uparrow$	1.066	1.091	0.982	0.798	<u>1.070</u>
BCEA- $s\uparrow$	1.327	1.964	1.365	1.230	<u>1.720</u>
BCEA- $n\downarrow$	0.0266	0.0008	0.0010	<u>0.0005</u>	0.0000

Table 1. Homogeneous image dehazing results on the RESIDE, HazeRD, O-HAZE and real-world datasets.

NTIRE'20	HLP	EPDN	MSBDN	FFA	TDN	Our
PSNR \uparrow	12.452	13.562	15.38	16.87	<u>23.06</u>	24.26
SSIM \uparrow	0.447	0.456	0.461	0.491	<u>0.755</u>	0.805
LPIPS \downarrow	0.697	0.689	0.710	0.715	<u>0.250</u>	0.199

Table 2. Non-homogeneous dehazing results on the NTIRE2020-Dehaze dataset.

NHR	MRP	OSFD	Our
PSNR \uparrow	19.93	28.74	31.03
SSIM \uparrow	0.777	0.947	0.977

Table 3. Nighttime dehazing results on the NHR dataset.

4.2.2 Non-Homogeneous Dehazing

We further evaluate our method on the non-homogeneous dehazing dataset NTIRE2020-Dehaze. Fig. 6 reveal the visual comparisons. As we can see, our model achieves the best visual quality and color contrast on NTIRE2020-Dehaze dataset. The quantitative results shown in Table 2 reveal that our model surpasses the second best methods by a very large margin, surpassing the second best methods 1.2 dB on PSNR, and 0.05 on SSIM, respectively. The reason is that the proposed HyLoG-ViT has a stronger ability in modeling long-range context information than the vanilla CNN.

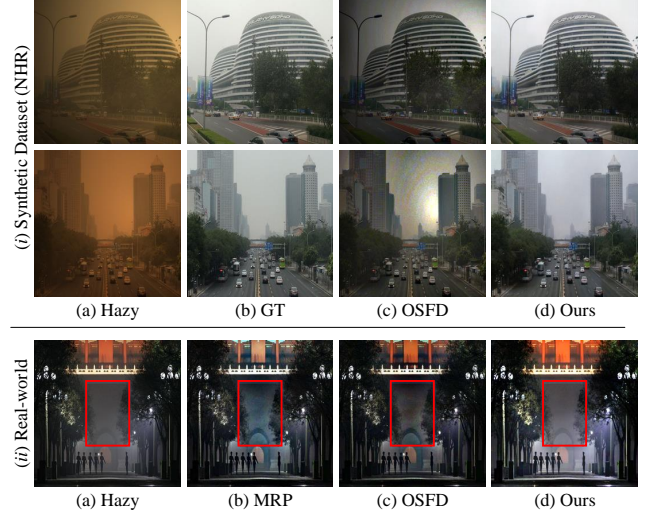


Figure 7. Visual results of nighttime dehazing.

4.2.3 Nighttime Dehazing

We further evaluate our dehazing model on the nighttime dehazing. The dehazing results tested on synthetic and real-world datasets are illustrated in Fig. 7 and Table 3. As we can find, our Transformer-based dehazing network leads to more visually realistic results than other methods (as regions highlighted by the red rectangles) both on the synthetic and the real-world nighttime hazy images. Moreover, the qualitative results also demonstrate that our model can perform surprisingly well on nighttime dehazing, outperforming the state-of-the-art MRP [44], and OSFD [45] methods with respect to PSNR and SSIM.

4.3. Discussion

Due to the stronger ability in modeling long-range context information, Transformer-based network structures are naturally good at learning the spatially variant features [40]. Our experiments verify this conclusion. The samples in the SOTS are synthetic by setting the atmospheric light and scattering coefficient as global constants. While in the O-HAZE and NTIRE2020-Dehaze datasets, hazy images are captured in natural scenes where the haze is generated by professional haze machines [2]. In fact, the atmospheric light and scattering coefficient will no longer be globally

	CNNs	ViT	L-ViT	G-ViT	LoG-ViT
PSNR↑	28.02	27.73	28.38	27.37	28.91
SSIM↑	0.953	0.940	0.958	0.947	0.959
	w/o-RS	w-R	w-S	w/o-CFSM	Our
PSNR↑	27.25	28.74	27.90	28.91	29.58
SSIM↑	0.942	0.951	0.960	0.959	0.962

Table 4. Results of the ablation studies.

constant in natural scenes under foggy and hazy conditions. Therefore, as shown in Table 1 and 2, our method can surpass the SOTAs by a very large margin on the O-HAZE and NTIRE2020-Dehaze; however, the four metrics of our method are not the best on the SOTS dataset.

4.4. Ablation Study

For quick experiments, all of the models are trained for 10 epochs and evaluated on 300 samples randomly selected from the SOTS [22] dataset in our ablation studies. The results are illustrated in Table 4.

4.4.1 Evaluations on the HyLoG-ViT

We evaluate the effectiveness of the proposed HyLoG-ViT model for image dehazing by involving the following different configurations, where the HyLoG-ViT block is replaced by: 1) two basic ResNet [18] blocks (CNNs); 2) the basic ViT block (ViT); 3) the local ViT path (L-ViT); 4) the global ViT path (G-ViT); 5) the sequential stacked local and global ViT paths (LoG-ViT). The model CNNs achieves better dehazing performance than the models of ViT, L-ViT, and G-ViT. One of the reasons is that Transformers-based models lack some of the inductive biases inherent to CNNs, such as translation equivariance and locality, and therefore do not generalize well when trained on insufficient data. Models of LoG-ViT and HyLoG-ViT obtain the top two PSNR and SSIM, indicating that combining local and global interactions are more effective than other models. Comparing them, we can find that our parallel hybrid scheme is better than the sequentially stacked one.

4.4.2 Evaluations on the Complementary Features

We further conduct the ablation studies to demonstrate the contribution of the joint model. 1) **w/o-RS**: our dehazing network without any complementary features, removing the decoders D_R and D_S ; 2) **w-R**: our dehazing model removing the decoder D_S ; 3) **w-S**: our dehazing model removing the decoder D_R . Comparing models of w/o-RS, w-R, and w-S, the latter two models obtain higher PSNR and SSIM than the former, indicating that the joint learning mechanism with complementary features of reflectance or shading indeed boosts the network’s dehazing performance. Fur-

thermore, when both complementary features are leveraged in our model, it achieves the best performance.

4.4.3 Evaluations on the CFSM

For checking the contribution of the CFSM, we conduct the experiment where the model **w/o-CFSM** refers to the dehazing model that with-out CFSM yet merge the complementary features d_R^z , d_S^z and features d_D^z by summation. The dehazing results are shown in the second row in Tabel 4. As we can find, without the CFSM, the dehazing results reduce 0.67 dB on PSNR and 0.003 on SSIM, indicating the importance and benefits of using the CFSM in the dehazing network.

5. Conclusion

In this paper, we introduce vision transformers into dehazing tasks. To this end, we design a new hybrid local-global vision transformer (HyLoG-ViT). The HyLoG-ViT is more computationally efficient than the standard ViT and can capture both local and global dependencies. Incorporating with the new vision transformer, we propose a new dehazing framework, which jointly learns the intrinsic image decomposition and dehazing. The reflectance and shading prediction tasks encourage the networks to learn more useful complementary features for image dehazing tasks. We propose a complementary features selection module to effectively aggregate those complementary features to enhance the useful complementary features while weakening the irrelevant ones. Extensive experiments on homogeneous, non-homogeneous, and nighttime dehazing tasks demonstrate that our method achieves comparable or even better performance than CNNs-based dehazing methods.

References

- [1] Codruta O Ancuti, Cosmin Ancuti, and Radu Timofte. Nh-haze: An image dehazing benchmark with non-homogeneous hazy and haze-free images. In *Proceedings of the Conference on Computer Vision and Pattern Recognition Workshop*, pages 444–445, 2020. 5, 16
- [2] Codruta O Ancuti, Cosmin Ancuti, Radu Timofte, and Christophe De Vleeschouwer. O-haze: a dehazing benchmark with real hazy and haze-free outdoor images. In *Proceedings of the Conference on Computer Vision and Pattern Recognition Workshop*, pages 754–762, 2018. 7, 15
- [3] Jimmy Lei Ba, Jamie Ryan Kiros, and Geoffrey E Hinton. Layer normalization. *arXiv preprint arXiv:1607.06450*, 2016. 6
- [4] Anil S Baslamisli, Thomas T Groenestege, Partha Das, Hoang-An Le, Sezer Karaoglu, and Theo Gevers. Joint learning of intrinsic images and semantic segmentation. In *Proceedings of the European Conference on Computer Vision*, pages 286–302, 2018. 2, 4

- [5] Dana Berman, Tali Treibitz, and Shai Avidan. Single image dehazing using haze-lines. *IEEE Transactions on Pattern Analysis and Machine Intelligence*, 42(3):720–734, 2018. 1, 3, 11
- [6] Bolun Cai, Xiangmin Xu, Kui Jia, Chunmei Qing, and Dacheng Tao. Dehazenet: An end-to-end system for single image haze removal. *IEEE Transactions on Image Processing*, 25(11):5187–5198, 2016. 2
- [7] Jianrui Cai, Shuhang Gu, and Lei Zhang. Learning a deep single image contrast enhancer from multi-exposure images. *IEEE Transactions on Image Processing*, 27(4):2049–2062, 2018. 5
- [8] Nicolas Carion, Francisco Massa, Gabriel Synnaeve, Nicolas Usunier, Alexander Kirillov, and Sergey Zagoruyko. End-to-end object detection with transformers. In *Proceedings of the European Conference on Computer Vision*, pages 213–229, 2020. 3
- [9] Hanting Chen, Yunhe Wang, Tianyu Guo, Chang Xu, Yiping Deng, Zhenhua Liu, Siwei Ma, Chunjing Xu, Chao Xu, and Wen Gao. Pre-trained image processing transformer. In *Proceedings of the IEEE Conference on Computer Vision and Pattern Recognition*, pages 12299–12310, 2021. 3, 11
- [10] Xiangxiang Chu, Zhi Tian, Yuqing Wang, Bo Zhang, Haibing Ren, Xiaolin Wei, Huaxia Xia, and Chunhua Shen. Twins: Revisiting the design of spatial attention in vision transformers. *arXiv preprint arXiv:2104.13840*, 1(2):3, 2021. 2, 3, 4
- [11] Xiangxiang Chu, Zhi Tian, Bo Zhang, Xinlong Wang, Xiaolin Wei, Huaxia Xia, and Chunhua Shen. Conditional positional encodings for vision transformers. *arXiv preprint arXiv:2102.10882*, 2021. 4
- [12] Keyan Ding, Kede Ma, Shiqi Wang, and Eero P Simoncelli. Image quality assessment: Unifying structure and texture similarity. *arXiv preprint arXiv:2004.07728*, 2020. 6
- [13] Hang Dong, Jinshan Pan, Lei Xiang, Zhe Hu, Xinyi Zhang, Fei Wang, and Ming-Hsuan Yang. Multi-scale boosted dehazing network with dense feature fusion. In *Proceedings of the IEEE Conference on Computer Vision and Pattern Recognition*, pages 2157–2167, 2020. 2, 3, 11
- [14] Jiangxin Dong and Jinshan Pan. Physics-based feature dehazing networks. In *Proceedings of the European Conference on Computer Vision*, pages 188–204. Springer, 2020. 1
- [15] Alexey Dosovitskiy, Lucas Beyer, Alexander Kolesnikov, Dirk Weissenborn, Xiaohua Zhai, Thomas Unterthiner, Mostafa Dehghani, Matthias Minderer, Georg Heigold, Sylvain Gelly, et al. An image is worth 16x16 words: Transformers for image recognition at scale. *Proceedings of the International Conference on Learning Representations*, 2020. 2, 3, 11
- [16] Raanan Fattal. Dehazing using color-lines. *ACM Transactions on Graphics (TOG)*, 34, 2014. 3
- [17] Kaiming He, Jian Sun, and Xiaoou Tang. Single image haze removal using dark channel prior. *IEEE Transactions on Pattern Analysis and Machine Intelligence*, 33(12):2341–2353, 2011. 1
- [18] Kaiming He, Xiangyu Zhang, Shaoqing Ren, and Sun Jian. Deep residual learning for image recognition. In *Proceedings of the IEEE Conference on Computer Vision and Pattern Recognition*, pages 770–778, 2016. 8, 11
- [19] Bela Julesz. Visual pattern discrimination. *IRE transactions on Information Theory*, 8(2):84–92, 1962. 2
- [20] Diederik P Kingma and Jimmy Ba. Adam: A method for stochastic optimization. In *Proceedings of the International Conference on Learning Representations*, 2015. 6
- [21] Diederik P Kingma and Pratul Dhariwal. Glow: Generative flow with invertible 1x1 convolutions. *arXiv preprint arXiv:1807.03039*, 2018. 6
- [22] Boyi Li, Wenqi Ren, Dengpan Fu, Dacheng Tao, Dan Feng, Wenjun Zeng, and Zhangyang Wang. Benchmarking single-image dehazing and beyond. *IEEE Transactions on Image Processing*, 28(1):492–505, 2018. 5, 8, 14
- [23] Jiafeng Li, Hong Zhang, Ding Yuan, and Mingui Sun. Single image dehazing using the change of detail prior. *Neurocomputing*, 156:1–11, 2015. 1, 3
- [24] Pengyue Li, Jiandong Tian, Yandong Tang, Guolin Wang, and Chengdong Wu. Deep retinex network for single image dehazing. *IEEE Transactions on Image Processing*, 30:1100–1115, 2020. 1, 2
- [25] Yawei Li, Kai Zhang, Jie Zhang Cao, Radu Timofte, and Luc Van Gool. Localvit: Bringing locality to vision transformers. *arXiv preprint arXiv:2104.05707*, 2021. 3
- [26] Jingyun Liang, Jie Zhang Cao, Guolei Sun, Kai Zhang, Luc Van Gool, and Radu Timofte. Swinir: Image restoration using swin transformer. *arXiv preprint arXiv:2108.10257*, 2021. 2, 3
- [27] Jing Liu, Haiyan Wu, Yuan Xie, Yanyun Qu, and Lizhuang Ma. Trident dehazing network. In *Proceedings of the Conference on Computer Vision and Pattern Recognition Workshop*, pages 430–431, 2020. 1, 5
- [28] Yunfei Liu, Yu Li, Shaodi You, and Feng Lu. Unsupervised learning for intrinsic image decomposition from a single image. In *Proceedings of the IEEE Conference on Computer Vision and Pattern Recognition*, 2020. 4, 5
- [29] Ze Liu, Yutong Lin, Yue Cao, Han Hu, Yixuan Wei, Zheng Zhang, Stephen Lin, and Baining Guo. Swin transformer: Hierarchical vision transformer using shifted windows. *arXiv preprint arXiv:2103.14030*, 2021. 3
- [30] Srinivasa G Narasimhan and Shree K Nayar. Vision and the atmosphere. *International Journal of Computer Vision*, 48(3):233–254, 2002. 2, 3
- [31] Muzammal Naseer, Kanchana Ranasinghe, Salman Khan, Munawar Hayat, Fahad Shahbaz Khan, and Ming-Hsuan Yang. Intriguing properties of vision transformers. *arXiv preprint arXiv:2105.10497*, 2021. 2
- [32] S.K. Nayar and S.G. Narasimhan. Vision in bad weather. In *Proceedings of the IEEE International Conference on Computer Vision*, volume 2, pages 820–827, 1999. 1
- [33] Xu Qin, Zhilin Wang, Yuanchao Bai, Xiaodong Xie, and Huizhu Jia. Ffa-net: Feature fusion attention network for single image dehazing. In *Proceedings of the Association for the Advancement of Artificial Intelligence*, pages 11908–11915, 2020. 6, 11

- [34] Yanyun Qu, Yizi Chen, Jingying Huang, and Yuan Xie. Enhanced pix2pix dehazing network. In *Proceedings of the IEEE Conference on Computer Vision and Pattern Recognition*, pages 8160–8168, 2019. 11
- [35] Wenqi Ren, Si Liu, Hua Zhang, Jinshan Pan, Xiaochun Cao, and Ming-Hsuan Yang. Single image dehazing via multi-scale convolutional neural networks. In *Proceedings of the European Conference on Computer Vision*, pages 154–169, 2016. 2, 3
- [36] Olaf Ronneberger, Philipp Fischer, and Thomas Brox. U-net: Convolutional networks for biomedical image segmentation. In *International Conference on Medical Image Computing and Computer-Assisted Intervention*, pages 234–241, 2015. 3
- [37] Yuanjie Shao, Lerenhan Li, Wenqi Ren, Changxin Gao, and Nong Sang. Domain adaptation for image dehazing. In *Proceedings of the IEEE Conference on Computer Vision and Pattern Recognition*, pages 2808–2817, 2020. 2
- [38] Ashish Vaswani, Prajit Ramachandran, Aravind Srinivas, Niki Parmar, Blake Hechtman, and Jonathon Shlens. Scaling local self-attention for parameter efficient visual backbones. In *Proceedings of the IEEE Conference on Computer Vision and Pattern Recognition*, pages 12894–12904, 2021. 2
- [39] Wenhai Wang, Enze Xie, Xiang Li, Deng-Ping Fan, Kaitao Song, Ding Liang, Tong Lu, Ping Luo, and Ling Shao. Pyramid vision transformer: A versatile backbone for dense prediction without convolutions. *Proceedings of the IEEE International Conference on Computer Vision*, 2021. 3
- [40] Zhendong Wang, Xiaodong Cun, Jianmin Bao, and Jianzhuang Liu. Uformer: A general u-shaped transformer for image restoration. *arXiv preprint arXiv:2106.03106*, 2021. 3, 7
- [41] Haiyan Wu, Yanyun Qu, Shaohui Lin, Jian Zhou, Ruizhi Qiao, Zhizhong Zhang, Yuan Xie, and Lizhuang Ma. Contrastive learning for compact single image dehazing. In *Proceedings of the IEEE Conference on Computer Vision and Pattern Recognition*, pages 10551–10560, 2021. 1, 3
- [42] Haiping Wu, Bin Xiao, Noel Codella, Mengchen Liu, Xiyang Dai, Lu Yuan, and Lei Zhang. Cvt: Introducing convolutions to vision transformers. *arXiv preprint arXiv:2103.15808*, 2021. 3
- [43] Enze Xie, Wenhai Wang, Zhiding Yu, Anima Anandkumar, Jose M Alvarez, and Ping Luo. Segformer: Simple and efficient design for semantic segmentation with transformers. *arXiv preprint arXiv:2105.15203*, 2021. 4
- [44] Jing Zhang, Yang Cao, Shuai Fang, Yu Kang, and Chang Wen Chen. Fast haze removal for nighttime image using maximum reflectance prior. In *Proceedings of the IEEE Conference on Computer Vision and Pattern Recognition*, pages 7418–7426, 2017. 7
- [45] Jing Zhang, Yang Cao, Zheng-Jun Zha, and Dacheng Tao. Nighttime dehazing with a synthetic benchmark. In *Proceedings of the ACM international conference on Multimedia*, pages 2355–2363, 2020. 1, 5, 7, 11, 17, 18
- [46] Richard Zhang, Phillip Isola, Alexei A Efros, Eli Shechtman, and Oliver Wang. The unreasonable effectiveness of deep features as a perceptual metric. In *Proceedings of the IEEE Conference on Computer Vision and Pattern Recognition*, pages 586–595, 2018. 6
- [47] Sixiao Zheng, Jiachen Lu, Hengshuang Zhao, Xiatian Zhu, Zekun Luo, Yabiao Wang, Yanwei Fu, Jianfeng Feng, Tao Xiang, Philip HS Torr, et al. Rethinking semantic segmentation from a sequence-to-sequence perspective with transformers. In *Proceedings of the IEEE International Conference on Computer Vision*, pages 6881–6890, 2021. 2, 3
- [48] Dongxiao Zhou. Human texture perception. <https://www.cs.auckland.ac.nz/~georgy/research/texture/thesis-html/node6.html>, 2006. Accessed: 2006-2-22. 2
- [49] Qingsong Zhu, Jiaming Mai, and Ling Shao. A fast single image haze removal algorithm using color attenuation prior. *IEEE Transactions on Image Processing*, 24(11):3522–3533, 2015. 1, 3

Supplementary Materials

6. More Discussions

6.1. Complexity Analysis

For the local ViT path, denote the input feature $X \in \mathbb{R}^{H \times W \times C}$ is grouped into $N_l \times N_l$ regions, and the spatial-resolution of each region is $\frac{H}{N_l} \times \frac{W}{N_l} \times C$. Then, the complexity of the self-attention in local ViT path is reduced from $O((HW)^2C)$ to $O(\frac{(HW)^2}{N_l^2}C)$ compared with the standard self-attention.

For the global ViT path, denote the spatial dimension of the input feature is down-scaled by a reduction ratio N_g , and the complexity is $O(\frac{(HW)^2}{N_g^2}C)$. Therefore, the total self-attention computational complexity of HyLoG-ViT block is $O((\frac{1}{N_l^2} + \frac{1}{N_g^2})(HW)^2C)$.

In our work, the $N_l = 8$ and $N_g = 4$, thus the total cost of the self-attention in HyLoG-ViT is $O(\frac{5}{64}(HW)^2C)$.

6.2. Position Encoding

In this experiment, we will show that, without the position encoding/embedding, our model can also achieve high performance on image dehazing. We also verify that the 3×3 convolution layer that fuses the hybrid features from local and global ViT paths is useful. Hence, we compared the following models: 1) **PE**: our HyLoG adds the learnable position encodings as used in [15, 9]; 2) **ADD**: the hybrid features are fused by element-wise summation. The quantitative results are shown in Table 5. As we can find, there are no significant performance gains to the SSIM when adding the position encoding. The PE model gets even lower the PSNR than Our model. However, the model of ADD performs worse than the other two models with respect to the PSNR and SSIM, demonstrating that the 3×3 convolution layer for hybrid features' fusion is vital in our HyLoG-ViT.

	PE	ADD	Our
PSNR↑	29.49	28.34	29.58
SSIM↑	0.963	0.955	0.962

Table 5. Ablation study results on the position encoding.

7. Architectures of the Encoder and Decoder

The encoder E is comprised of a feature extraction layer and a series of HyLoG-ViT blocks. The extraction layer is built by a 5×5 convolution, and a basic ResNet block [18] to extracts shallow features. Each HyLoG-ViT block is followed by a 4×4 convolution to downscale the spatial resolution with stride 2 and double the channel number. The convolutions used here can bring the inductive bias into the Transformer-based encoder.

In the decoder D_R and D_S , except the bottom stage Z , feature $d_{R/S}^{z-1}$ from the previous decoder block is first up-scaled by a 4×4 deconvolution to expand the spatial resolution with stride 2 and halve the channel number. Then, the output is concatenated with the feature e^z from the same stage of encoder E . Therefore, the subnetworks $E - D_R$ and $E - D_S$ are formed into two U-shaped structures, which can alleviate the issue of spatial information loss caused by downscaling. Different from decoder D_R and D_S , for z -th stage in D_D , there have three inputs, the features d_D^{z-1} from previous stage, d_R^z and d_S^z from the same stage of D_R and D_S , respectively. These input features are feed into a complementary features selection module (CFSM) to dynamically select the most useful complementary feature channels from d_R^z and d_S^z .

8. More Results (High-resolution)

We compare our model with other methods and conduct extensive experiments, including *homogeneous, non-homogeneous, nighttime* and *low-light* hazy image dehazing, to verify the effectiveness of it. The compared methods include HLP [5], EPDN [34], MSBDN [13], FFA [33] and OSFD [45]. Please refer to the next page.

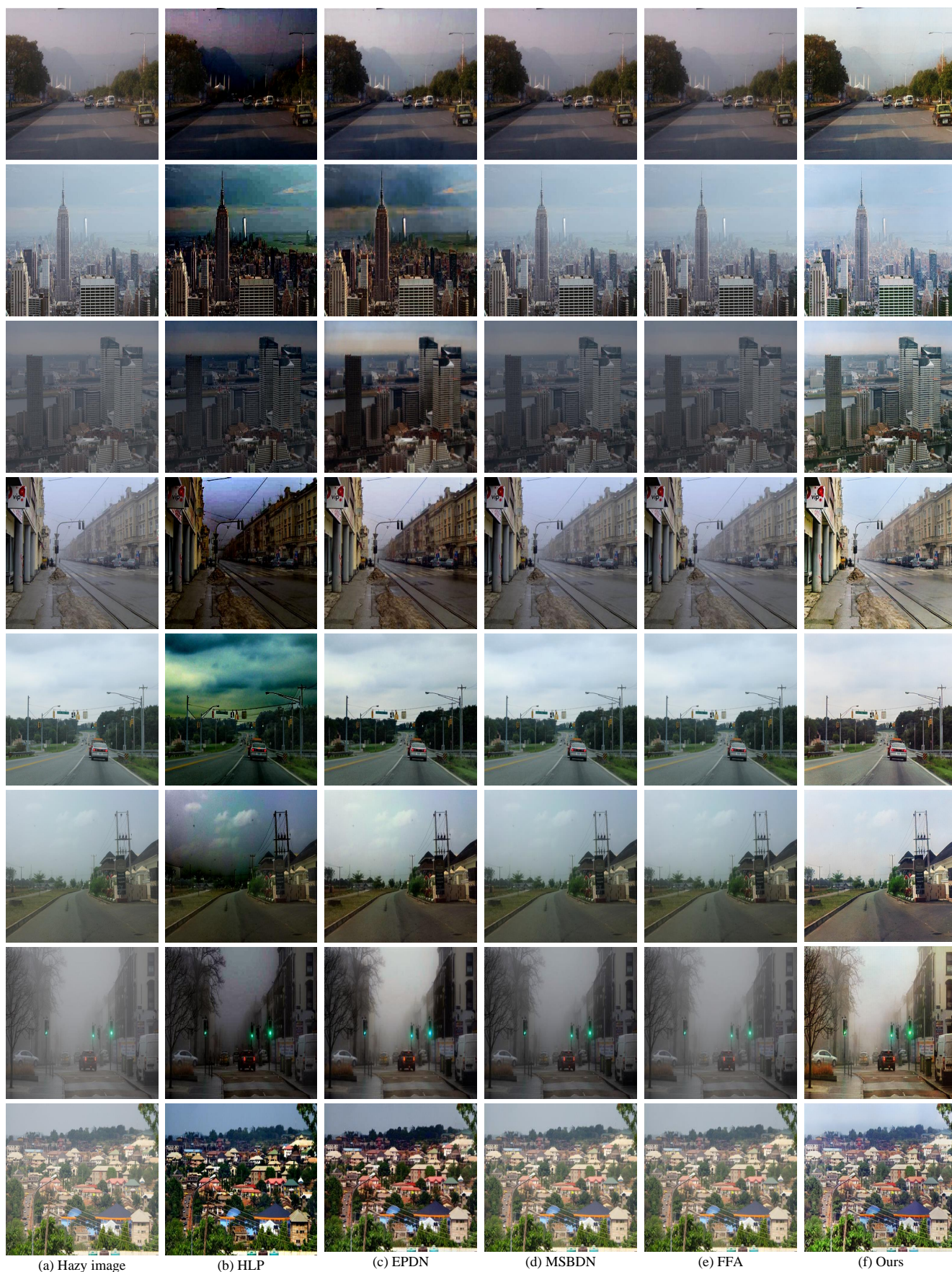


Figure 8. High-resolution visual results of homogeneous dehazing (Real-world datasets).

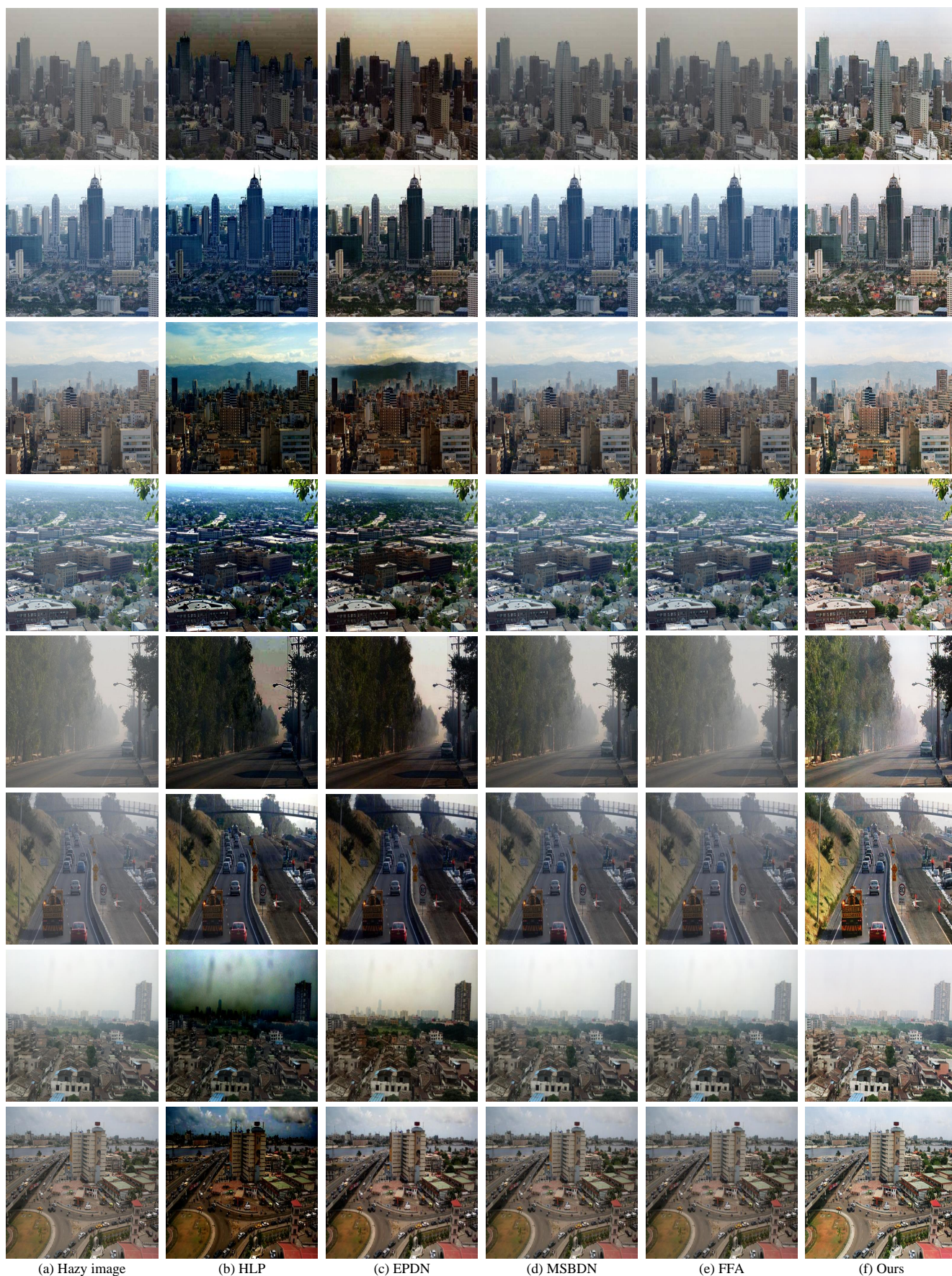


Figure 9. High-resolution visual results of homogeneous dehazing (Real-world datasets).



(a) Hazy image

(b) HLP

(c) EPDN

(d) MSBDN

(e) FFA

(f) Ours

(g) GT

Figure 10. High-resolution visual results of homogeneous dehazing (SOTS dataset [22]).



Figure 11. High-resolution visual results of homogeneous dehazing (O-HAZE dataset [2]).



Figure 12. High-resolution visual results of non-homogeneous dehazing (NTIRE2020-Dehaze dataset [1]).



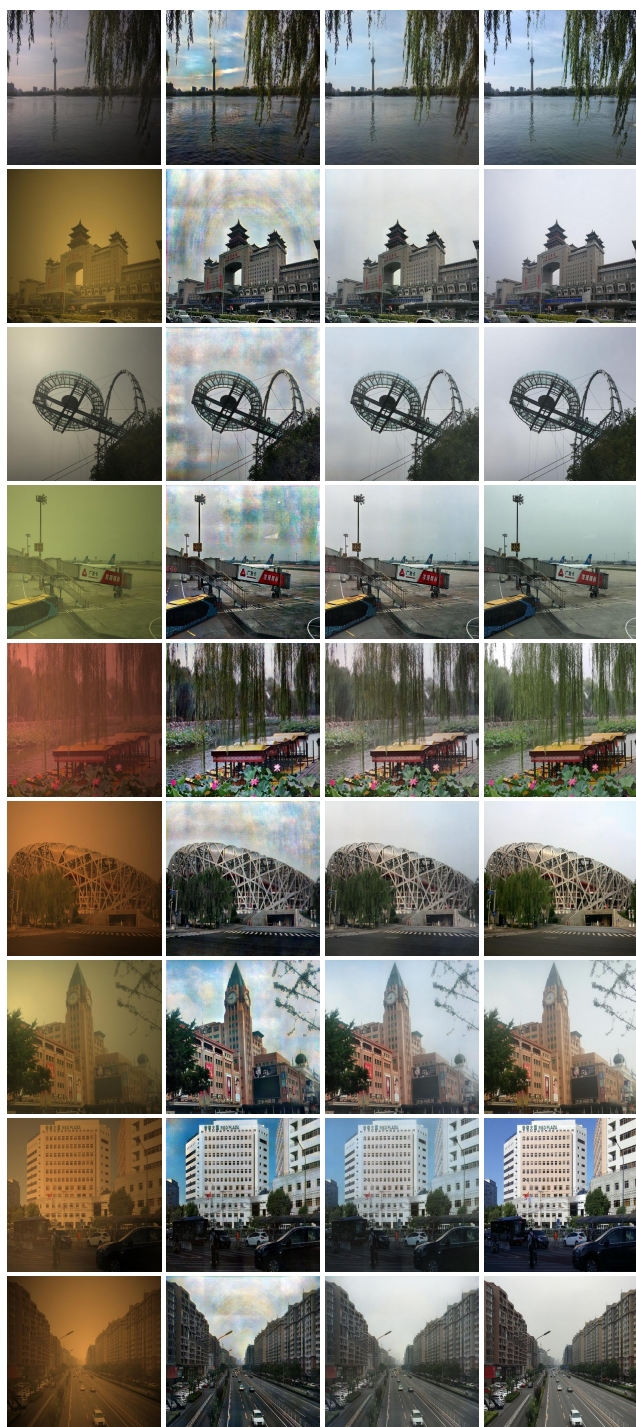
(a) Hazy image (b) OSFD (c) Ours

Figure 13. High-resolution visual results of nighttime dehazing (NHRW dataset [45]).



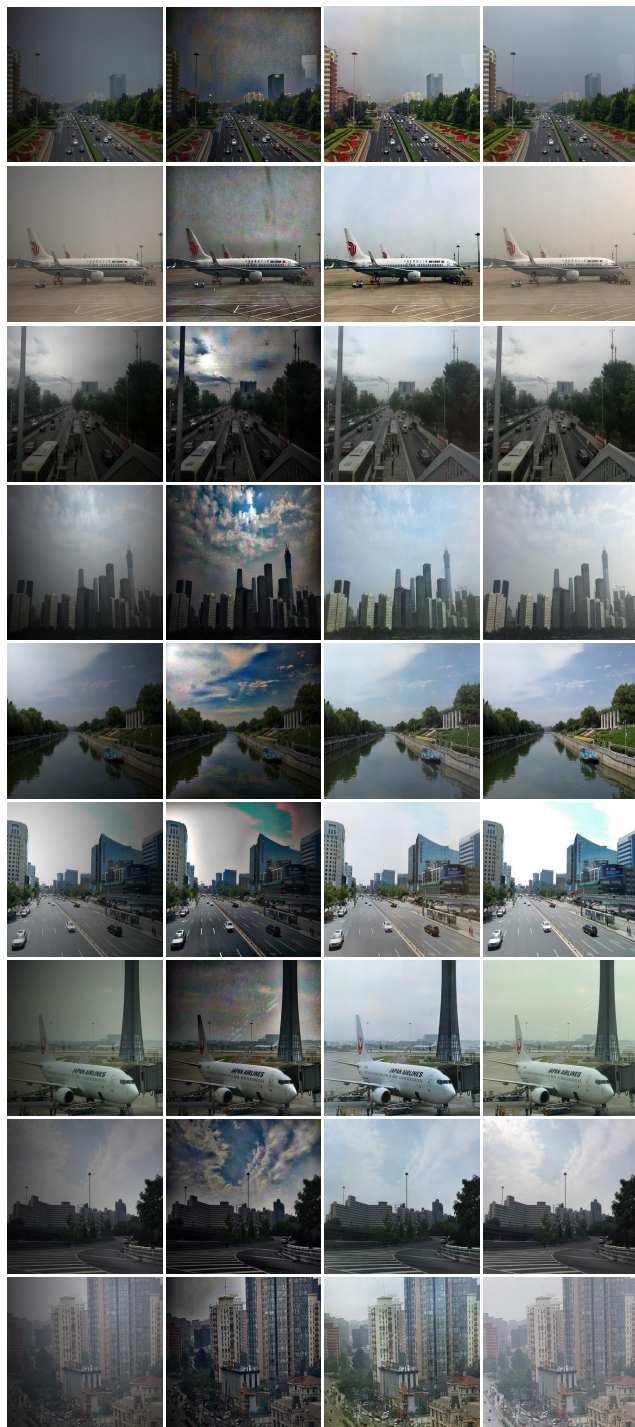
(a) Hazy image (b) OSFD (c) Ours

Figure 14. High-resolution visual results of nighttime dehazing (NHRW dataset [45]).



(a) Nighttime Hazy Image (b) OSFD (c) Ours (d) GT

Figure 15. High-resolution visual results of nighttime dehazing (NHR dataset [45]).



(a) Low-light image (b) OSFD (c) Ours (d) GT

Figure 16. High-resolution visual results of low-light image dehazing (NHR dataset [45]).

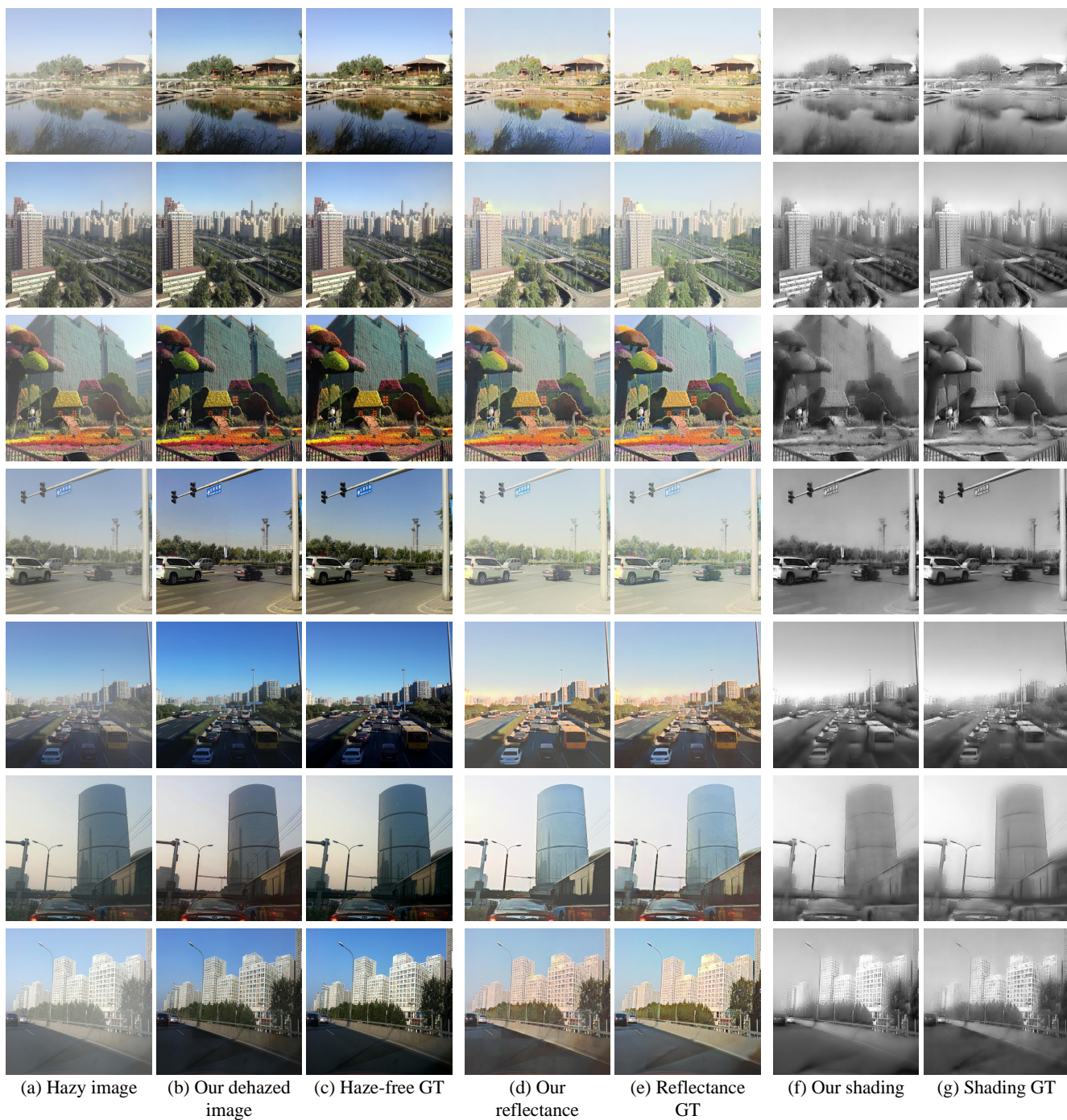


Figure 17. High-resolution visual results of intrinsic image decomposition.